Available online at www.sciencedirect.com
ScienceDirect
Journal of volcanology and geothermal research
Journal of Volcanology and Geothermal Research 165 (2007) 127–141
www.elsevier.com/locate/jvolgeores

Recent lahars at Volcán de Colima (Mexico): Drainage variation and spectral classification

N. Davila [a], L. Capra [b,*], J.C. Gavilanes-Ruiz [c], N. Varley [d], G. Norini [b], Angel Gómez Vazquez [e]

[a] *Posgrado en Geografía, UNAM, CU, 40510 Coyoacán, México D.F., México*
[b] *Centro de Geociencias, Campus Juriquilla, UNAM, 76230 Queretaro, México*
[c] *Centro Universitario de Investigaciones en Ciencias del Ambiente, Universidad de Colima, Km. 9 Carretera, Colima-Coquimatlán, Coquimatlán 28400, Colima, Mexico*
[d] *Facultad de Ciencias, Universidad de Colima, Av. 25 de Julio #965, Colima, Col. CP 28045, México*
[e] *Centro Nacional de Prevención de Desastres (CENAPRED), Mexico D.F., Mexico*

Received 15 November 2006; received in revised form 29 March 2007; accepted 17 May 2007
Available online 5 June 2007

Abstract

Volcán de Colima is the most active volcano in Mexico, and represents a high risk for more than 500,000 people. In 1998 the volcano renewed its activity, with the extrusion of a lava dome and subsequent lava and block and ash flows. During the recent period of activity pyroclastic products did not directly affect villages around the volcano, however, several lahars did.

We used LIDAR topographic coverage, ASTER and LANDSAT images for the recognition of morphological changes in the drainage system and lahar detection. For lahar delineation we applied principal components analysis and canonical classification (Tasseled Cap) in order to perform a supervised image classification using the maximum likelihood rule algorithm. LAHARZ (objective delineation of distal debris flow hazard zones) has been used and tested using two topographic datasets with different resolutions, which provided evidence of the importance of high-resolution topographic coverage in hazard assessment. Finally a hazard map for lahars is presented, showing that several villages and ranchos can be affected. In contrast, due to morphological changes produced by products of the intense explosive activity, other populated areas such as La Yerbabuena, are outside of the high risk zone. They could be affected by lahars only in case of cataclysmic eruptions such as the 1913 Plinian event.

Keywords: Volcán de Colima; lahar; ASTER; LANDSAT; hazard map

1. Introduction

Volcán de Colima is currently the most active volcano in Mexico (Fig. 1). Since 1998 intermittent activity has been observed with Vulcanian eruptions, lava flows and growing domes that have collapsed producing several block-and-ash flow deposits (Saucedo et al., 2002, 2004, 2005). Pyroclastic flows did not reach long distances, most of the time less than 5 km from the crater, however in some cases evacuation was considered necessary. In contrast, rain-induced lahars were more frequent and reached long distances, causing damage to infrastructure and being able to affect small villages such as La Becerrera in 2000.

* Corresponding author.
E-mail address: lcapra@geociencias.unam.mx (L. Capra).

0377-0273/$ - see front matter © 2007 Elsevier B.V. All rights reserved.
doi:10.1016/j.jvolgeores.2007.05.016

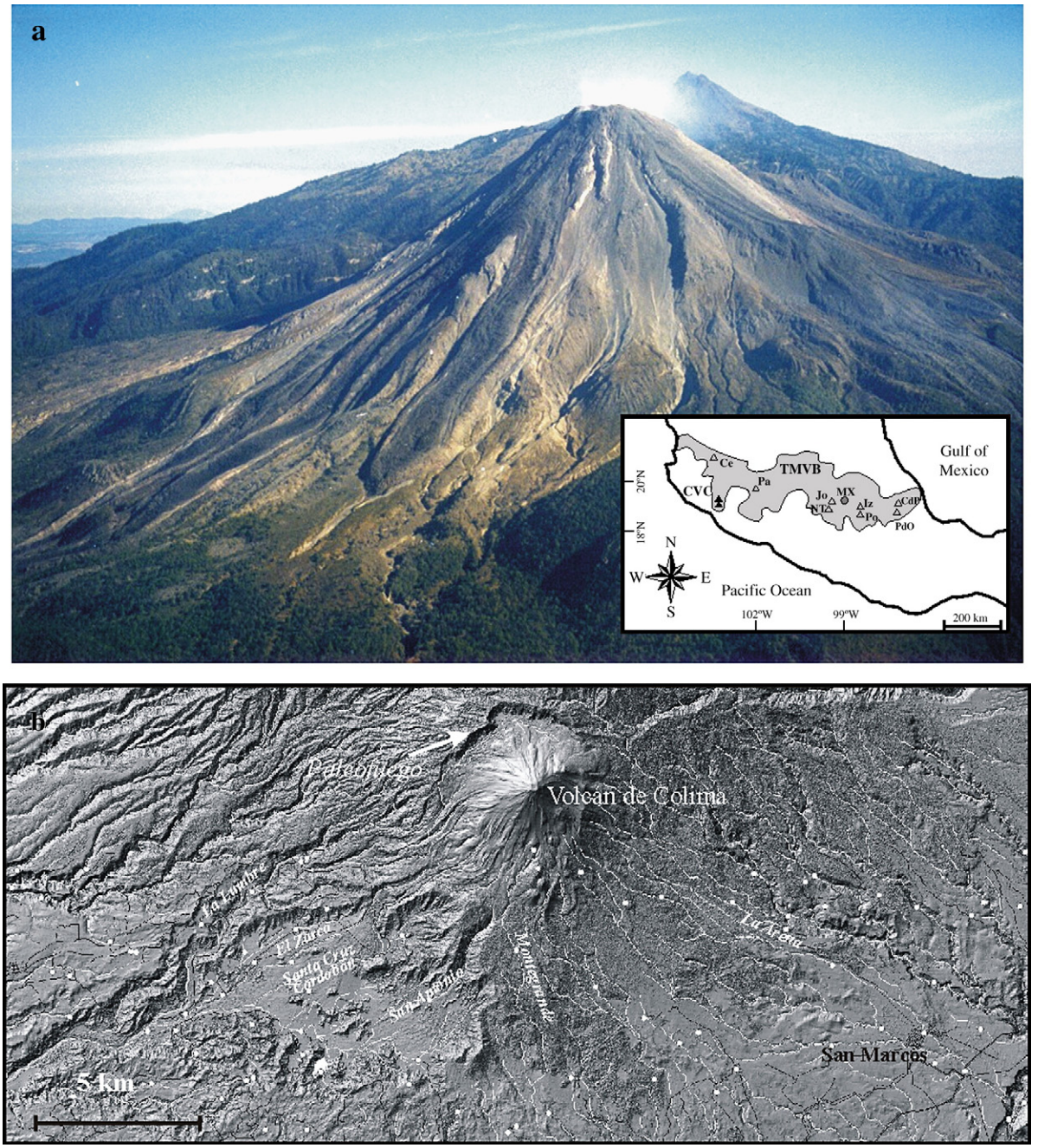

Fig. 1. a) Panoramic view from S of Volcán de Colima, where it is possible to observe the recent lava and pyroclastic flow deposits. The inset shows the location of the volcano in the Trans-Mexican Volcanic Belt (TMVB). Abbreviations are: CVC: Colima Volcanic Complex; Ce: Ceboruco; Pa: Paricutin; NT: Nevado de Toluca; Jo: Jocotitlán: MX: Mexico City; Iz: Iztacihuatl; Po: Popocatepetl; PdO: Pico de Orizaba; Cdp: Cofre de Perote. b) DEM of the Volcán de Colima showing the horse-shoe-shaped caldera where the currently active cone has been built and main ravines on its southern sector.

The aim of the present work is to study how the drainage system has changed during the last 15 yr of activity and which ravines are more susceptible to the erosive process forming lahars. ASTER and LANDSAT images were used for spatial and spectral delineation of recent lahars coupled with field data and high resolution Digital Elevation Models (DEM). Finally, the LAHARZ program is used to delineate possible lahar inundation zones but also to show the importance of high-resolution topographic coverage in hazard assessment.

2. Terminology and methodology

Lahar is a general term for rapidly flowing water-saturated mixture of rock debris and water from a volcano (Smith and Fritz, 1989). In most common cases heavy rains are the most common triggering mechanism, but other sources for the water are possible, such as the rupture of crater lakes (Manville et al., 1999), temporary volcanic dams (Capra, in press), and glacial water outburst (Gudmundsson et al., 1998). Depending upon the sediment concentration, different types of debris flow can be formed and gradually transform to hyperconcentrated flow (Scott, 1988). In the present work, when describing the images we will generically refer to lahars to include all such types of flows, since their behavior here is not taken into account for their delineation or spectral classification.

Two different DEMs were obtained from two topographic data sets, one from a topographic map with 10 m contour lines based on aerial photos of 1995 (from this point named as 1995-DEM), and a second one from LIDAR (Light Detection and Ranking) data taken in 2005 from which a 5 m DEM have been obtained (2005-DEM). All vectorial data were provided by INEGI (Instituto Nacional de Estadística Geografía e Informática). The DEMs where analyzed with ArcGis 9.1 program (using the Hydrology tools of the Spatial Analysis extension) to obtain the hydrological network and to compare how they changed from 1995 to 2005. It is worth mentioning that the 5 m DEM obtained from the 1995 topography does not have the same quality as the 2005 Lidar version since the first one was obtained interpolating 10 m contour lines, while the second by processing digital information that had a 30 cm resolution. Despite this disparity, a meaningful comparison could be made, as showed in the next sections.

For spatial and spectral delineation LANDSAT and ASTER images were used and processed. Cloud-free ASTER images of March, 2001 and April, 2006 were processed and compared also with an ETM LANDSAT image taken in December 1999 and one TM LANDSAT image of March 1990. ASTER images were acquired at the USGS Glovis system, while the LANDSAT are from the free download site of the Global Land Cover Facility

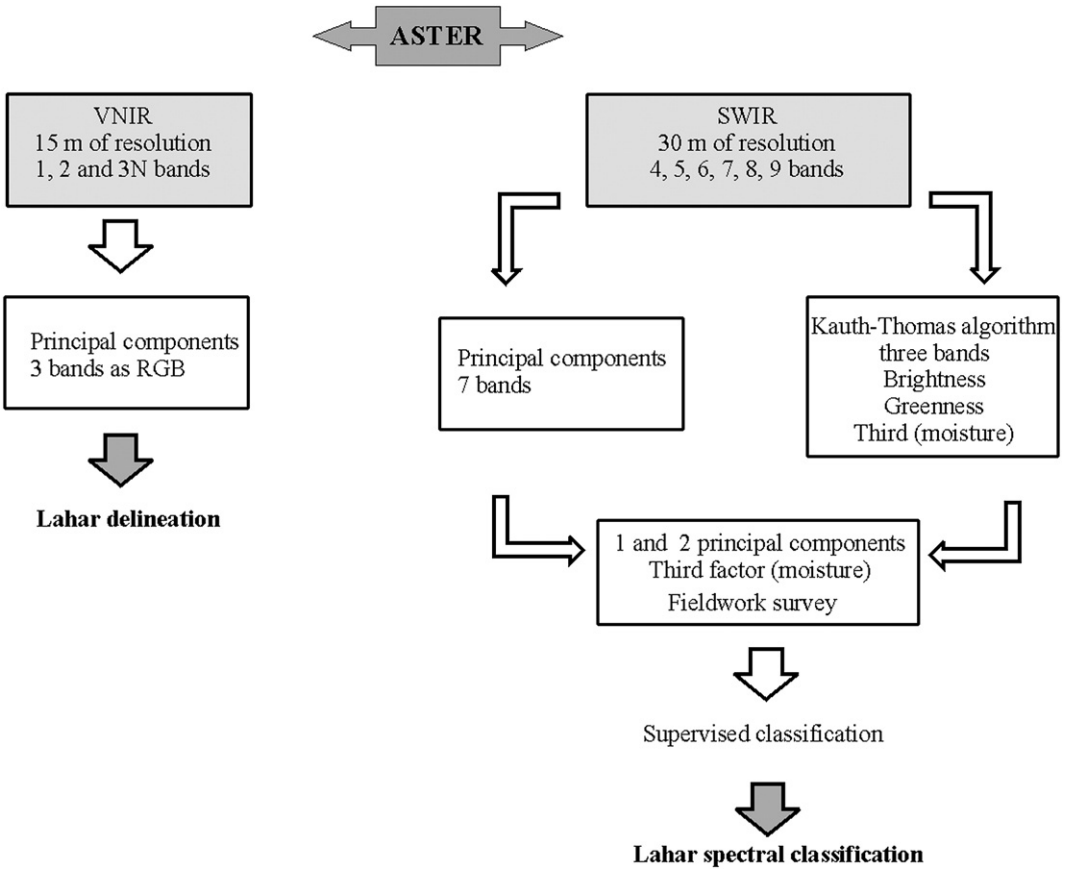

Fig. 2. Flow diagram showing the methodology used for spatial and spectral classification of lahar deposits based on ASTER images.

of University of Maryland (http://glcf.umiacs.umd.edu/index.shtml). The flow-diagram of Fig. 2 summarizes the methodology used. For spatial lahar delineation we used the VNIR (Visible Near-Infrared) 1 (0.52–0.60 μm), 2 (0.63–0.69 μm) and 3N (0.78–0.86 μm) bands for their higher spatial resolution (15 m) and because the combination of their three principal components gave the best results. In contrast, for spectral analysis and classification we used the SWIR (Short-Wave Infrared) subsystem (30 m resolution) because of the higher number of bands (with higher spectral resolution), which are more appropriate to distinguish geological patterns and vegetation. The SWIR spectrum composed of bands from 4 to 9 (1.60–1.70; 2.145–2.185; 2.185–2.225; 2.235– 2.285; 2.295–2.365; 2.360–2.430 μm respectively) was used to obtain the principal components. Then the Tassled Cap transform (also known as the Kauth-Thomas algoritm, Kauth et al., 1979) was applied. This consists of a canonical analysis that generate an orthogonal transformation of the original data into a new three-dimensional space consisting of the Brightness, Greenness, and Third indices, where this last one is related to soil features, including moisture status. The Tasseled Cap vegetation index was proposed for TM LANDSAT image data for analysis of vegetation, and it is here adapted to the VNIR and SWIR subsystem-ASTER (after an appropriated spectral equivalence) to try to exclude the vegetation contribution (the Greenness index) from the spectral classification and to enhance the lahars deposits with the Third index. This procedure it is based on the assumption that even if block-and-ash and lahar deposits are made of the same components, their moisture degree should be different. In this sense the Third index should contribute to enhance images of recent lahars in the main ravines. The spectral classification was made based on a supervised classification using the maximum likelihood rule which defines classes from the statistics of the image itself. The classes are defined by an operator, who chooses representative areas of the scene to define the mean values of parameters for each recognizable class (i.e. lahars and pyroclastic flow based on field work.). The likelihood classification rule assumes that these probabilities are equal for all classes and that the input bands have a normal distribution. Here we used the two first principal components coupled with the Third index in order to obtain a composite image for the spectral classification.

Finally, the LAHARZ routine was used to construct a hazard map. This is a semi-empirical model, designed as a rapid, objective and reproducible automated method for mapping areas of potential lahar inundation (Schilling and Iverson, 1998). The method employs the result of scaling and statistical analyses of the geometry of several lahars and debris flows in order to predict downstream inundation areas as a function of volume. Two empirical equations were extrapolated from the observation of 27 cases: $A=0.05\ V^{2/3}$ and $B=200\ V^{2/3}$, where A is the maximum inundated cross-sectional area, B is the total planimetric area of inundation and V is the volume of the lahar. The input to apply the routine is a DEM of the area and an estimation of flow volumes, which can be from direct calculation in the field (using for example the super-elevation method or flow traces

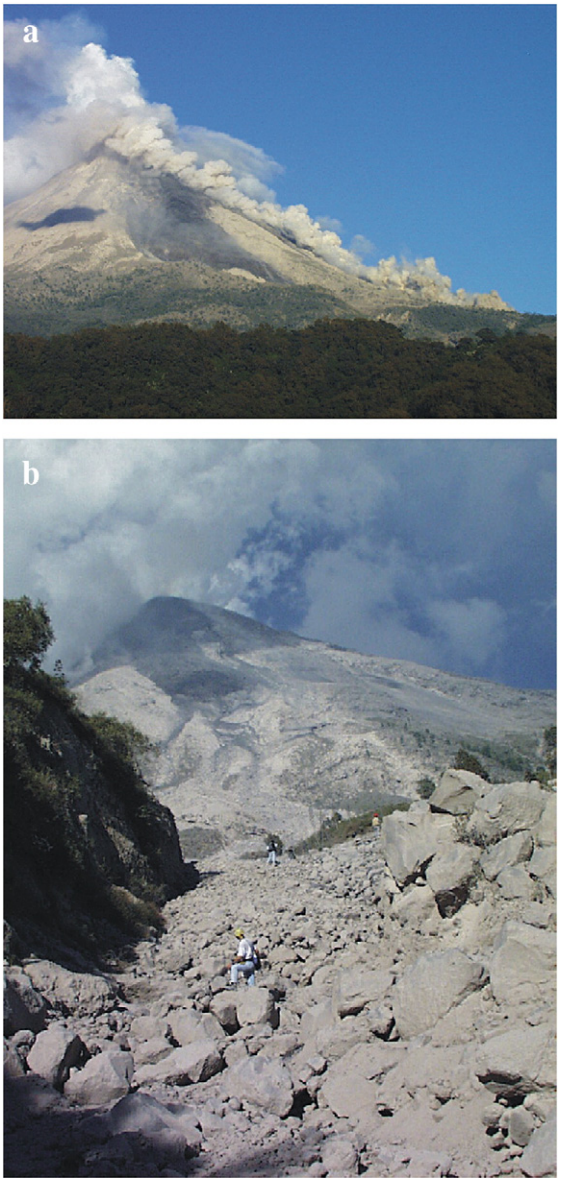

Fig. 3. a) Panoramic view of a pyroclastic flow originated from a dome collapse; b) Lateral levee of a pyroclastic flow on its proximal outcrop (picture courtesy of J.L. Macías).

on tree) but can also be reiterated from the program based on the observed maximum runout of the flow. In the present work we will apply this method by using both 1995-DEM and 2005-DEM, showing the importance of having a high resolution DEM to get more reliable results, as previously noted by Stevens et al. (2002).

3. Recent activity at Volcán de Colima

Volcán de Colima, also known as Volcán de Fuego, is 3860 m high and represents the younger cone of the Colima Volcanic Complex, located in the western limit of the Trans-Mexican Volcanic Belt (Fig. 1a). It consists of an andesitic composite cone, ~50 ka in age (Robin et al., 1987), which has been the locus of several sector collapses. Komorowski et al. (1997) proposed up to nine collapse events, with the younger occurring probably at 4280 yr BP (Luhr and Prestegaard, 1985), but this topic is still controversial (Robin et al., 1987; Komorowski et al., 1997). Paleofuego, the ancestral edifice, presents a southward horse-shoe-shaped caldera where the currently active cone has been built (Fig. 1b). During the past centuries the volcano has experienced different eruptive styles, from Merapi or Soufriere dome collapse, to Vulcanian and Plinian eruptions (Saucedo et al., 2005). After the 1913 plinian activity, the volcano presented several eruptive phases, each one lasting a few years, but since 1998 its activity has become more persistent with Vulcanian eruptions and lava and dome extrusion (Saucedo et al., 2005). Recent effusive episodes have occurred in 1991, 1998–9, 2001–3 and 2004; with major explosive events in 1994, 1999, 2003 and 2005. Activity has been continuous since 2001, with several explosions occurring daily between the periods of effusive eruptions. During this period, the partial collapse of Vulcanian eruptive columns, as well as the collapse of summit domes and lava flows fronts, produced several block-and-ash flow deposits that filled proximal drainages up to distances of 6 km from the vent (Fig. 3) with thickness up to several meters in the proximal area. The largest pyroclastic flow known to have occurred since 1913 resulted from a partial collapse of the dome on the NW side during October 2004. This partially filled La

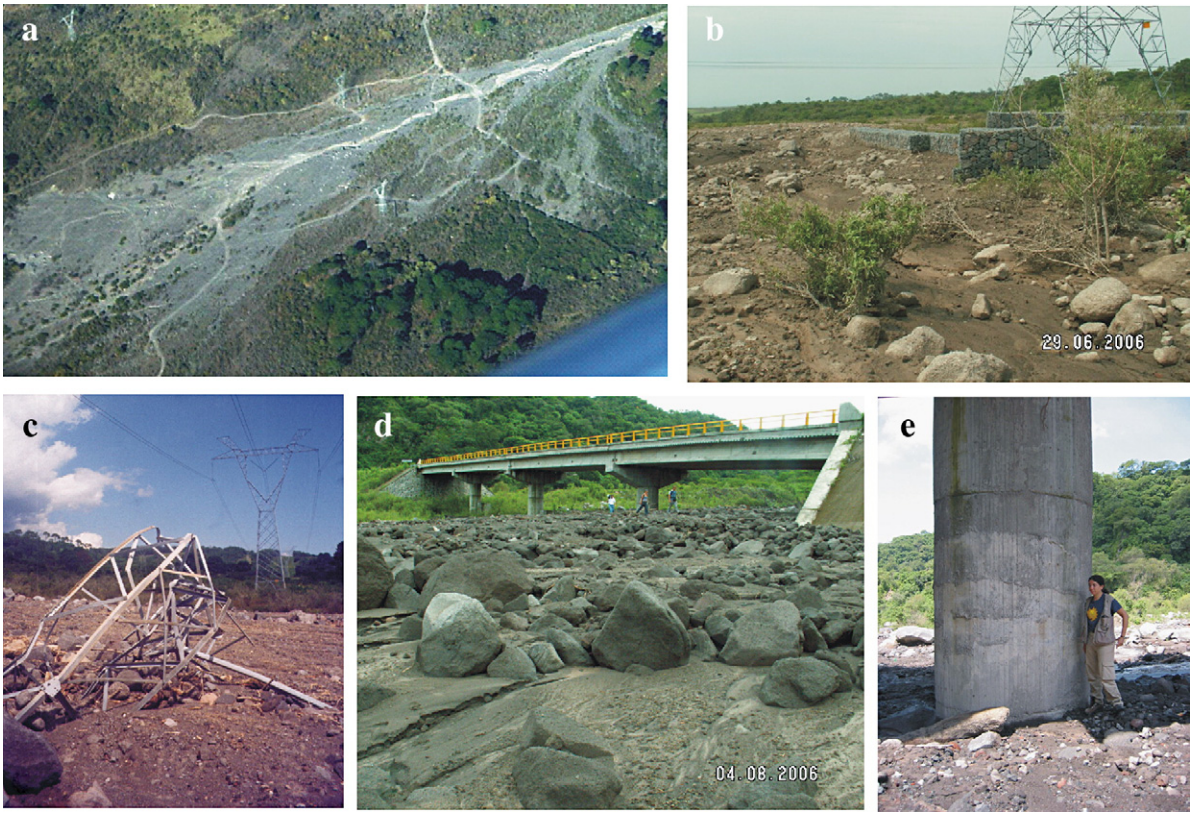

Fig. 4. Photos showing the several examples of damages provoked by lahars. a, b and c) Aerial view of the 1999 lahar in the Montegrande ravine where electric lines have been destroyed, note that the electric lines are now protected by a small rock barrier. d and e) Bridge over La Lumbre ravine where lahars charged with metric-sized blocks partially damaged the structure.

Lumbre ravine to a distance of 6.3 km from the crater. In the period February to September 2005 at least 19 pyroclastic flows occurred, this time as a result of column collapse. The largest distances were reached in the Montegrande and La Arena ravines, where the flows reached a maximum distance of 5.4 km. An initial estimation of the volume of the deposits resulting from these flows is $>6*10^6$ m^3. The block-and-ash flows at Colima volcano consist of an unwelded deposit with clasts embedded in a silty–sandy matrix.

Despite this intense eruptive activity, the emitted products have not significantly affected the inhabited area. In contrast, during the rainy season, which usually occur from June through to October at this latitude after a period of dryness, these deposits are easily remobilized as lahars. In particular, annual precipitation in the Colima area is around 1500 mm, with maximum pick of 500 mm during July (data source from Comision Nacional del Agua at http://smn.cna.gob.mx/). As a consequence, during July lahar are more frequents and with grater magnitude. The eruption occurred on 17th July 1999 ended with the emplacement of a voluminous block-and-ash flow deposit that filled the San Antonio and Montegrande ravines (Saucedo et al., 2002; Sarocchi, 2006). The day after the event, heavy rains remobilized part of this pyroclastic flow within the Montegrande ravine forming a lahar that destroyed an electric power line (Figs. 1b, and 4). The year after, on July 1st, 2000, along El Zarco and La Lumbre ravines, after approximately one hour of heavy rains a mayor lahar occurred that partially buried two houses. The bridge over La Lumbre ravine that connects La Becerrera with San José del Carmen (Puente Rio La Lumbre) was also affected (Figs. 1b and 4d and e). Under these climatic conditions, water easily removes deposited material and bulks to debris flows able to transport meter-sized clasts over

Fig. 5. Photo showing lahar deposits at Volcán de Colima. a) Upper portion of the Montegrande ravine, 15 m wide, prior to its opening where the main fan formed and b) outcrop of a lahar formed on June 28, 2006. c) La Arena ravine with a lahar deposit emplaced in 2005 and d) detail of the deposit where it is possible to observe a coarse, clast-supported basic layer and a normally graded upper layer.

long distances, inundating and provoking damage to infrastructure such as bridges. Generally the lahar deposit shows a clast supported base (flow head) topped by a more dilute layer, sometimes normally graded (body and tail of the flow) (Fig. 5), typical texture of such type of flows (Pierson and Scott, 1985; Rodolfo and Arguden, 1991; Major et al., 1996; Lavigne and Thouret, 2002). Finally they dilute to stream flow further from the source. More detailed textural and sedimentological work is now in progress.

Currently no sophisticated system for lahar detection is in operation at Volcán de Colima. The volcano seismic network operated by RESCO (Red Sísmica de Colima) consists of four short-period seismometers and one broad-band instrument located to the N, SW and SE of the volcano at distances of between 1.9 an 8 km from the summit. The seismic records are used to identify the occurrence of lahars, to have some idea of their relative size and which ravine they descended, however, it is not clear what theresold of debris flow provokes seismicity that can be detected above the background noise. During the period 2004–6, 57 lahars were detected in the Montegrande and La Lumbre ravines. Fig. 6 shows these events with the duration defined by the period when seismicity was produced in excess of the background noise level. It is worth mentioning that, due to the lack of direct visual observation of these ravines, some of these events do not necessarily corresponded to "bulked" lahars, but only to short water discharge with high clast concentration, as usually observed in the volcano, where large blocks up to 70 cm in diameters roll on the river bed during heavy rains without bulking to lahars. In addition, the durations here represented are only indicative of the signal that can be distinguished from the noise, probably corresponding with the peak discharge of the flow, meaning that the total lahar duration should be higher. Despite this limitation, the purpose of these diagrams is to show that again July represents the month during which lahar are more frequents, and that larger duration events occurred in 2005. This was a reflection of the increase in volume of the pyroclastic deposits available for remobilization by the rains. Fig. 7 shows the significant increase in lahar activity from 2005 to 2006. No data are available for previous years to extend this comparison.

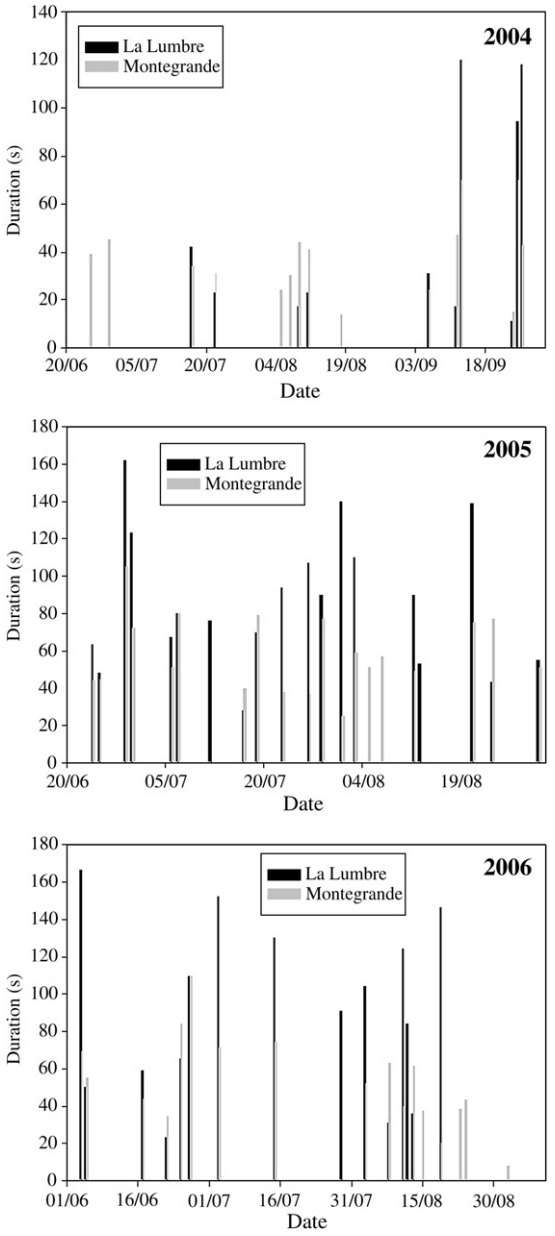

Fig. 6. Duration of individual lahar events at Volcán de Colima during 2004, 2005 and 2006. The duration has been determined from the seismic record from two stations located relatively close to the Montegrande and La Lumbre ravines, the two principally active ravines for lahars during recent years. (Data for 2006 is to the end of August).

4. Drainage system

The lava and pyroclastic flows emplaced during the last years of activity changed the drainage system on the volcano. Since the current edifice of Volcán de Colima is located within a horse-shoe-shaped caldera facing south, the drainage on its southern flank is subject to higher gradients meaning it is more susceptible to erosion. The continuous deposition of pyroclastic flow material during recent years on the southern flank periodically filled the drainage channels. Subsequently the deposits have been gradually eroded during the formation of lahars. A mean distribution of the lava and pyroclastic flow deposits was obtained by subtracting the 1995-

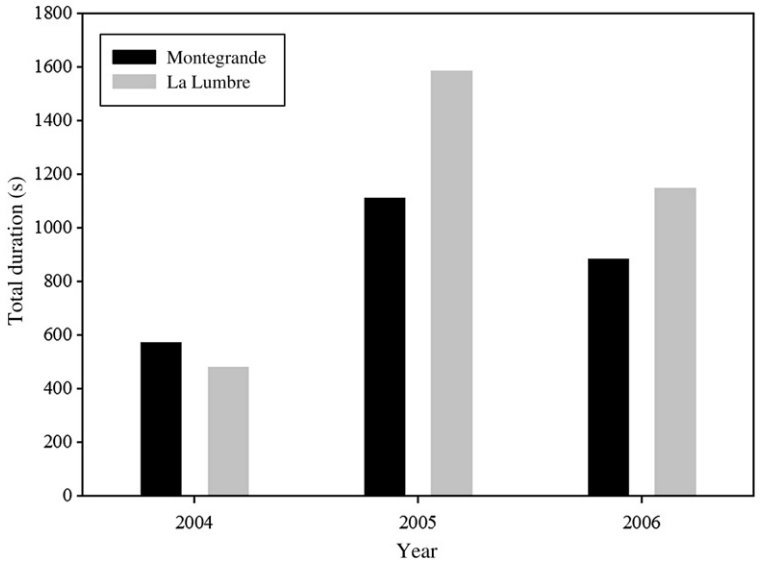

Fig. 7. Total duration of lahars in the two principal ravines of Montegrande and La Lumbre for the years 2004–6. Duration is based upon recorded seismicity. (Data for 2006 is to the end of August).

DEM from the 2005-DEM (Fig. 8a), and this distribution is used to better understand how the drainage has deviated. Despite the difference in DEM resolutions, by comparing the 1995 and 2005 flow networks and the pyroclastic flow distribution, it is clear that the deposits deviated and obliterated some of the drainage channels (Fig. 8a). Even if most of these changes are due to the resolution of the DEMs, especially in the lower part of the cone, the purpose of this comparison is to show that the system had became "younger" by the intense pyroclastic flow deposition and it is now eroding upslope again. The topographic section of Montegrande ravine shows how the slope changes. From the summit of the volcano up to a distance of 1.6 km, where a main brake in slope occurs, channels are 10 m wide with maximum gradient of 32° (Fig. 8b). From this point the topographic gradient becomes gentler, from 19–11° at ~5 km to 7° at a distance of ~10 km where the river channel is up to 20 m wide. From this point the slope gradually decreases from 4° up to 2° on the alluvial fans and the channel widens from 40 m up to 100 m, as also observable in the aerial view on Fig. 4a. None of these drainages are perennial, except for the La Lumbre one.

5. Spatial delineation and spectral classification of lahars

For Volcán de Colima we used two LANDSAT images of March 1990 and December 1999 and two ASTER images, taken in March 2001 and in April 2006. Fig. 9 compares the LANDSAT images that differ by approximately 10 years. These two images represent the scenario of the volcano before and after 10 years of activity. By comparing the two LANDSAT images, it is obvious that since 1991 the explosive activity has covered the entire cone with its products. Several ravines appear to be deeply eroded in the 1999 image where it is possible to observe lahars in the main drainage except for the Cordobán and Montegrande ravines that also show activity in the 1990 image. In particular, in the 1999 LANDSAT image the lahar in the Montegrande ravine that destroyed the electric line is easily recognizable.

For lahar delineation ASTER images were used, and as previously explained only the VNIR 1, 2 and 3N band were used. Fig. 10 shows the representation of the three principal components in RGB colors, where lahars are easily recognizable in an orange tone in the main ravines. It is possible to identify lahar activity in the following ravines: La Lumbre, El Zarco, Santa Cruz-Cordobán, San Antonio, Montegrande and La Arena. For the San Antonio and Montegrande drainages it was possible to delineate two main fans formed by lahars and observe their variation from 2001 to 2006 (Fig. 10). This comparison is evidence that throughout these five years these ravines remained active but that the magnitude of the lahars did not change significantly. This is an important issue since it indicates that Volcán de Colima has maintained its eruptive style. Lahars have been frequent but greatly reduced in magnitude when compared to lahars associated with cataclysmic eruptions (Stoopes and Sheridan, 1992; Komorowski et al., 1997; Capra and Macías, 2002). The hazard map presented in

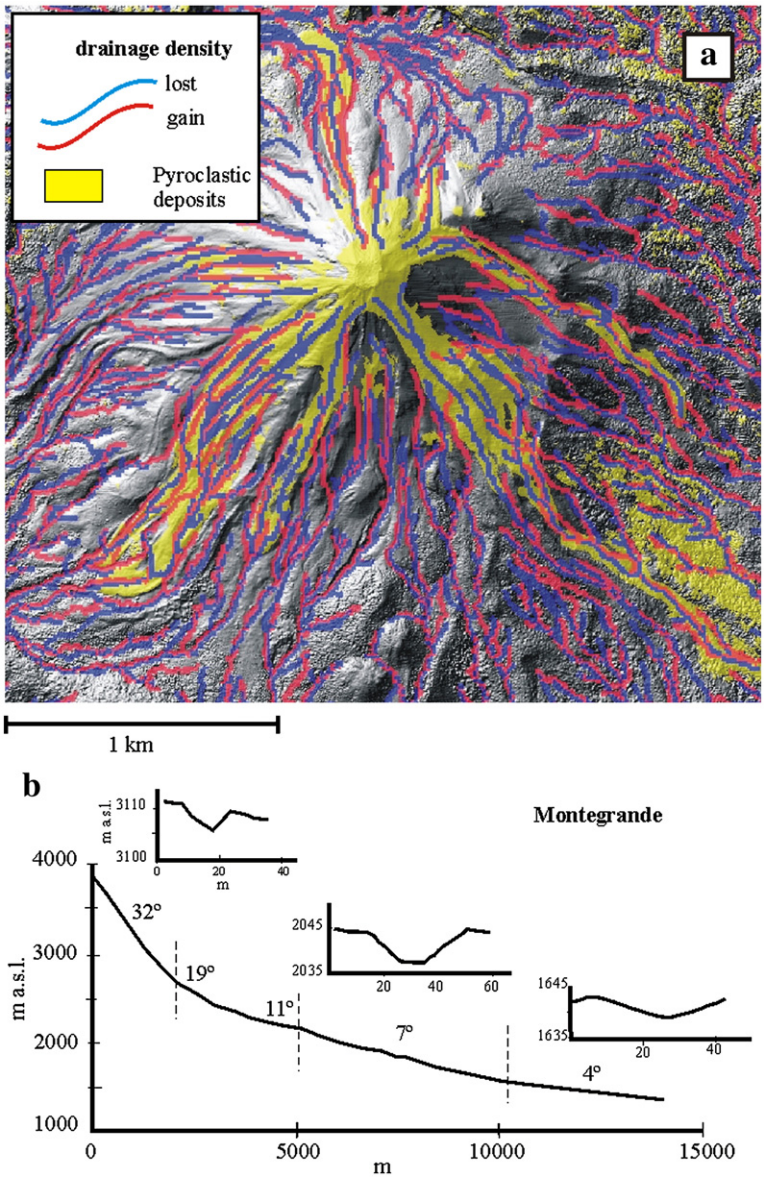

Fig. 8. a) Comparison between the drainage network of 1995 and 2005 with respect to the distribution of pyroclastic deposits. Note the disappearances where pyroclastic and lava flow were emplaced within the drainage channels; b) Topographic section along Montegrande ravines showing how the slope gradient and channel width change.

the next paragraph attempts to delineate the hazard inundation limit for such a type of rain induced lahar.

The morphometric and spatial analysis of Volcán de Colima previously described clearly show how the drainage changed and which ravines are the most active for lahar formation. For this case study we propose an objective lahar spectral classification in order to identify all recent events by a spectral pattern, to distinguish them from the primary pyroclastic deposits, and finally use the distribution to prepare a hazard map. The first two principal components of the SWIR spectrum contain the higher degree of information. In particular, the second component seems to have the best information about the lahars as showed in Fig. 11. For example, by combining this component with the brightness and the third index of the Kauth–Thomas algorithm (excluding the Greenness factor that represents the vegetation index) lahars are again easily distinguishable (Fig. 11). These kinds of combinations are appropriate for classifying the image and obtain a unique spectral response for lahars.

The problem for Volcán de Colima is that the origin of lahars is the remobilization of block-and-ash flow

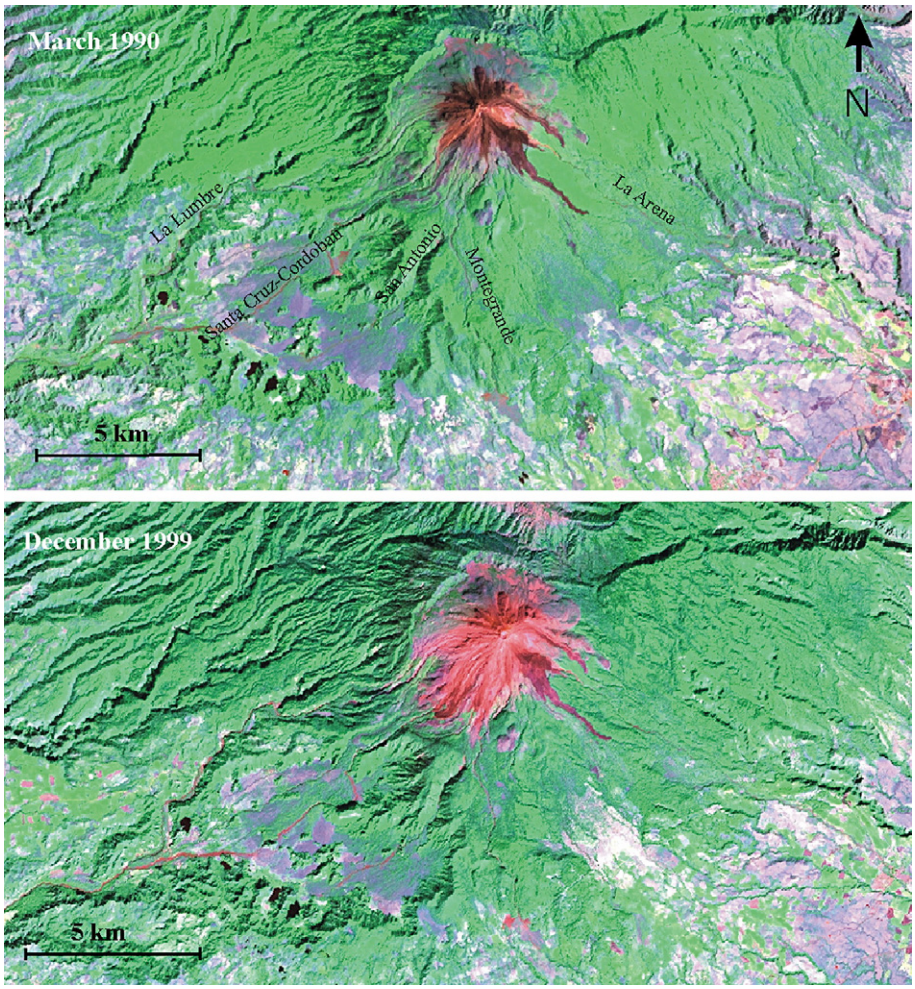

Fig. 9. Comparison between 1990 and 1999 LANDSAT images (4, 5 and 7 bands in RGB combination), showing that the cone has been completely covered by pyroclastic deposits and that main ravines are deeply eroded.

deposits, which implies that their spectral response can by very similar. In fact, from Fig. 11 it is evident that the material on the surface of the cone is similar to that recognizable in the drainage channels, here identified as lahars. The only parameter that can distinguish these lahar deposits from the pyroclastic flows is their degree of water saturation, since granulometric differences cannot be determined with such image resolution. For this reason the spectral classification was carried out using only the "Third" index from the K–T algorithm, which indicates the degree of soil moisture coupled with the first two principal component of the SWIR spectrum, as previously detailed in the methodology. In addition, the classification was supervised, which means that the known lahars inundation limits obtained by field observation were used to calibrate the classification.

Fig. 12 show the image obtained by the supervised classification where it is possible to identify by the dark-blue color the lahars along the main ravines and in dark red and green tones the pyroclastic flow deposits on the uppermost part of the cone. This classification can partially discriminate between pyroclastic flow and lahar deposits. In fact, there is a more extensive blue area between the pyroclastic flow deposit and the channeled lahars that probably corresponds to the transitional zone where water from heavy rains starts to infiltrate and saturate fresh pyroclastic deposits causing lahars initiation. In fact, this blue area stars approximately at the main break in slope of the cone, at approximately 2 km from the crater, where slope change from 39° to 19° (Fig. 8b). But again, since compositionally the block-and-ash flow and lahar deposits are similar, it is very difficult to separate them in the image in this transitional area, which can be an identifier to the source of lahar. Despite this uncertainty, the main objective here is to determine the maximum runout and

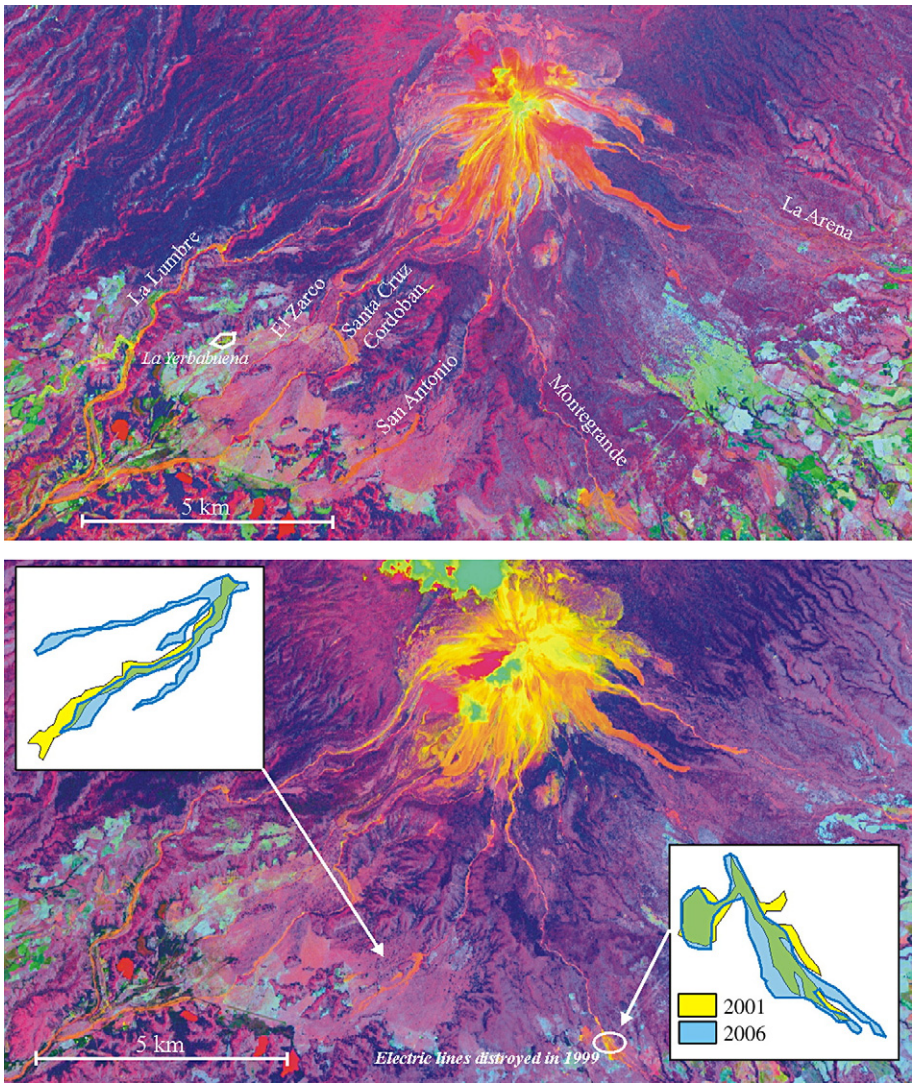

Fig. 10. From top to bottom: principal components of the VNIR spectrum of the 2001 and 2006 ASTER images (as RGB combination). Note that lahars are easily recognizable in an orange tone. In the insets, two fans on San Antonio and Montegrande ravines are compared.

possible inundation limit of lahars, to produce a hazard map. Due to the low resolution of the SWIR spectrum (30 m) the lahar traces are not continuous. As showed before, the width of the ravines can be less than 30 m and in such cases it is impossible to classify lahars. The other classes identified in the image of Fig. 12 have been established based on the geological map of Volcán de Colima (Cortés Cortés et al., 2005) such as the debris avalanche unit. Other undifferentiated classes refer to other old volcanic deposits, probably debris avalanche, but here considered using a generic term since they do not influence our classification. In contrast, cultivated areas are easily distinguishable from lahars; a very important factor because due to associated moisture degree they can be mistaken for lahar deposits.

6. Hazard zonation

The lahar events here described can be considered of low magnitude but of high frequency, with various events occurring during the rainy season. Although in recent years these lahars have not caused injuries to people, they caused damage to bridges, electric lines and some other infrastructure. A hazard map for such a type of event can be useful for Civil Protection during the hurricane season. To construct this map the LAHARZ application (Iverson et al., 1998) was used to simulate the inundations limit based on the flow volume obtained from some studied events (Gavilanes-Ruiz, 2004) but also extrapolated from the LAHARZ program itself for the event where only the maximum runout was known

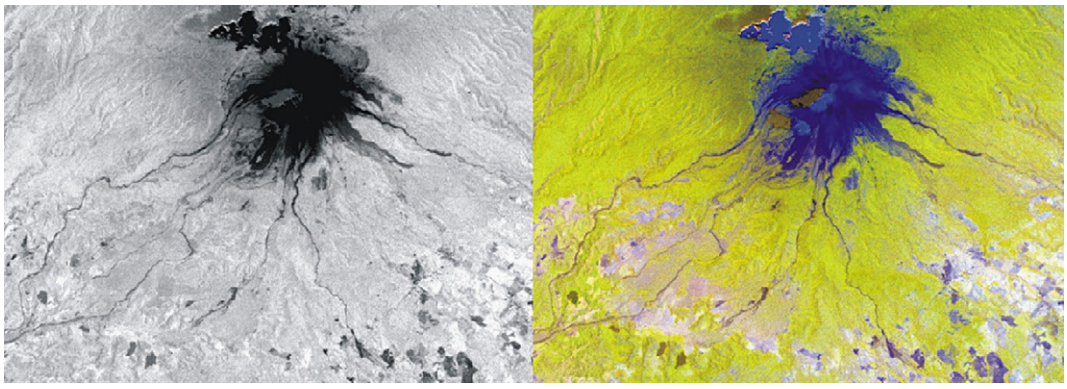

Fig. 11. Second principal component (left) and image obtained by the combination of the first and the second component plus the Third band of the Kauth–Thomas algorithm (Third index and 1 and 2 principal components in RGB colors). Note that lahars can be easily distinguished within the main ravines but are similar to the block-and-ash-flow deposit covering the cone.

or deducted from the spatial and spectra delineation here presented, which range between 8 and 10 km from the source The values used were 500,000 m^3, 250,000 m^3, 100,000 m^3 and 50,000 m^3. The simulations were performed with both topographic coverages, to test the program with DEMs with different resolutions. Finally, the hazard map was produced for the most active ravines as here identified by spatial and spectral analyses, and with the LIDAR coverage not only because of its high resolution, but also because, as previously mentioned, the drainage system had changed since 1995 and some ravines are no longer active.

Fig. 13 shows the inundation limits obtained for the Montegrande ravine with both sets of topographic data. The more evident difference between the two simulations is that the runout distance for the 2005 DEM is higher; however, the lateral inundation is reduced. This difference is more evident in Fig. 14, where three sections have been obtained at the same distance for both DEMs. The maximum inundation limit is highly variable with values more than four times higher for the 1995-DEM (i.e. section a, MIL from 59 m for the 2005-DEM to 199 m for the 1995-DEM). As a consequence, since the A value of LAHARZ representing the area of the flow

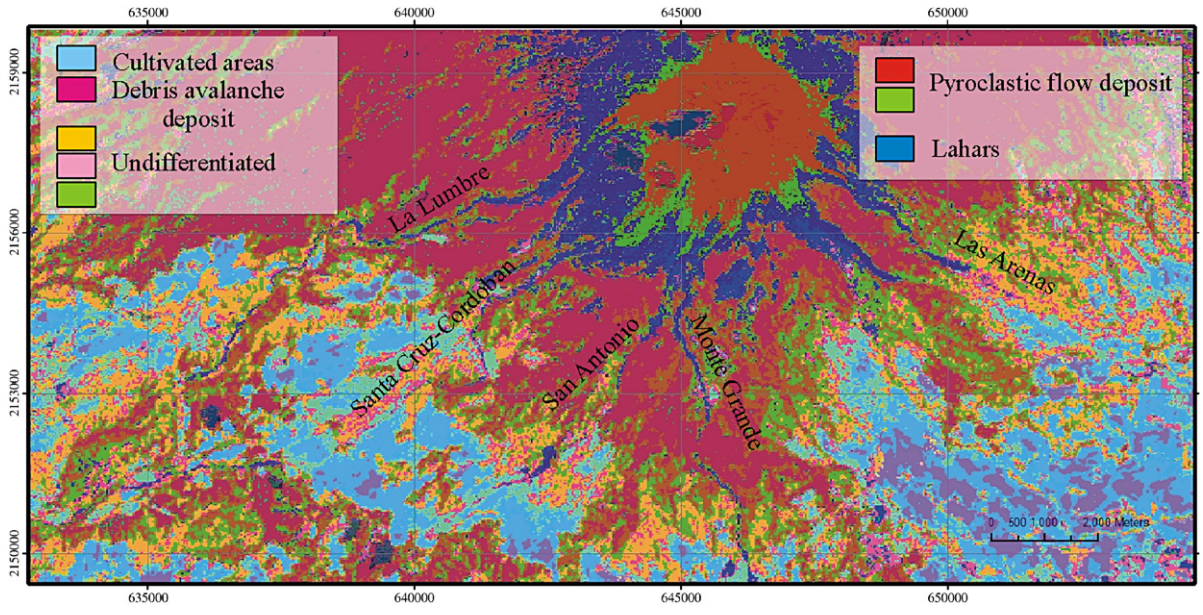

Fig. 12. Supervised classification of the studied area. Note that lahars can be distinguished in the dark-blue color from the pyroclastic flow deposit as red-light green.

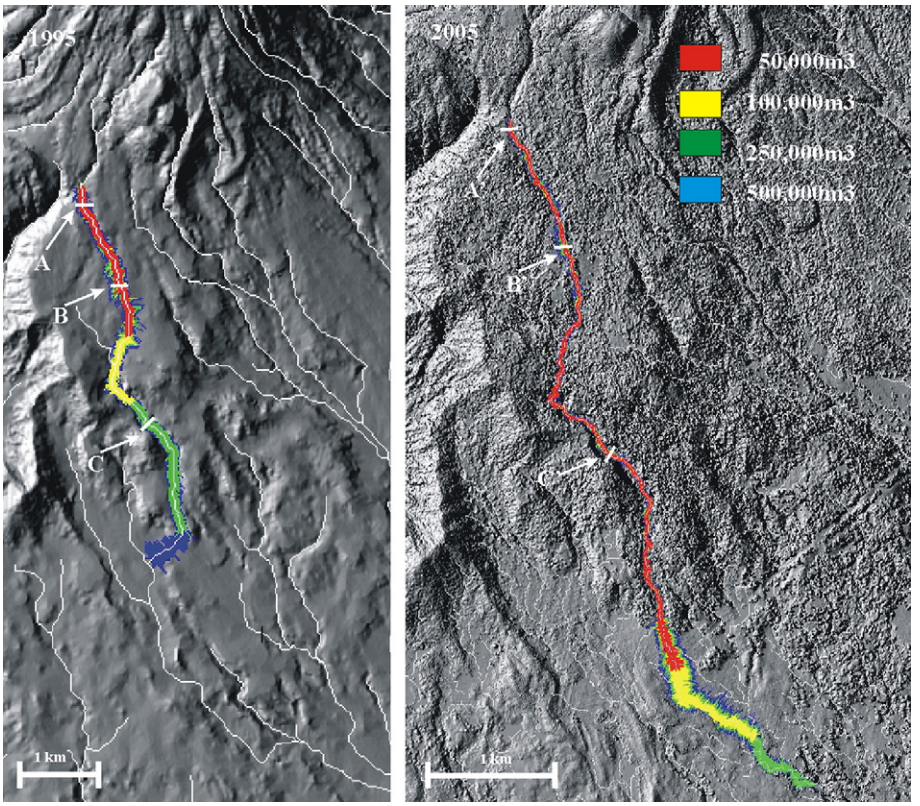

Fig. 13. Simulation of the inundation area using the 1995-dem (left) and the 2005-DEM (right). Note that for the same simulated flow volumes, the runout is greater with a more detailed DEM.

section is constant, the flow thickness will increase in the 2005 DEM, but in this case the difference is not so exaggerated. This disparity between the two simulations can be explained considering that the 1995 DEM was generated with a 1:50,000 topographic map, for which the interpolation will generate a smoothed morphology with respect to the 2005 LIDAR data where the original data have a resolution of 30 cm. As a consequence, when using the 1995 DEM the flow simulation will easily run up laterally producing higher inundation limits and therefore bigger flow sections; however, the simulation will stop early giving a shorter runout. For the 2001 Montegrande lahar, whose volume has been estimated at 200,000 m^3 (Gavilanes-Ruiz, 2004), its extension observable in the ASTER image is quite similar to the distribution obtained by the simulation with the LIDAR topography using a volume between 100,000 m^3 and 250,000 m^3 (Fig. 13). In contrast, to obtain the same distribution with the 1995 DEM a volume of approximately 600,000 m^3 would have been necessary.

The final hazard map (Fig. 15) obtained with the 2005 DEM indicates that various examples of infrastructure could be affected by lahars including bridges, electric lines as well as some small villages such as San Marcos, San Antonio or La Becerrera (seriously affected by lahars in 2000) and several ranches such as El Jabalí, Hotel Mahakua, Laguna La María touristic area, and Pedro Virgen Schulte, important infrastructure for the economy of the region. In contrast, La Yerbabuena village, which is one of the first places to have been evacuated during past activity and has been subject of a re-location, is not susceptible to lahar inundation, since the river no longer turns westward as it did probably more than 10 years ago. Only debris flows with a very large volume could bifurcate and reach La Yerbabuena village, which could only result from cataclysmic activity such as the 1913 Plinian eruption, which would occur with a catastrophic effect and produce many hazards besides lahars.

7. Conclusions

The analysis presented here helped to identify the most active ravines at Volcán de Colima for lahars. Easily available ASTER images can be a good tool to quickly identify such kind of phenomena on an active volcano and

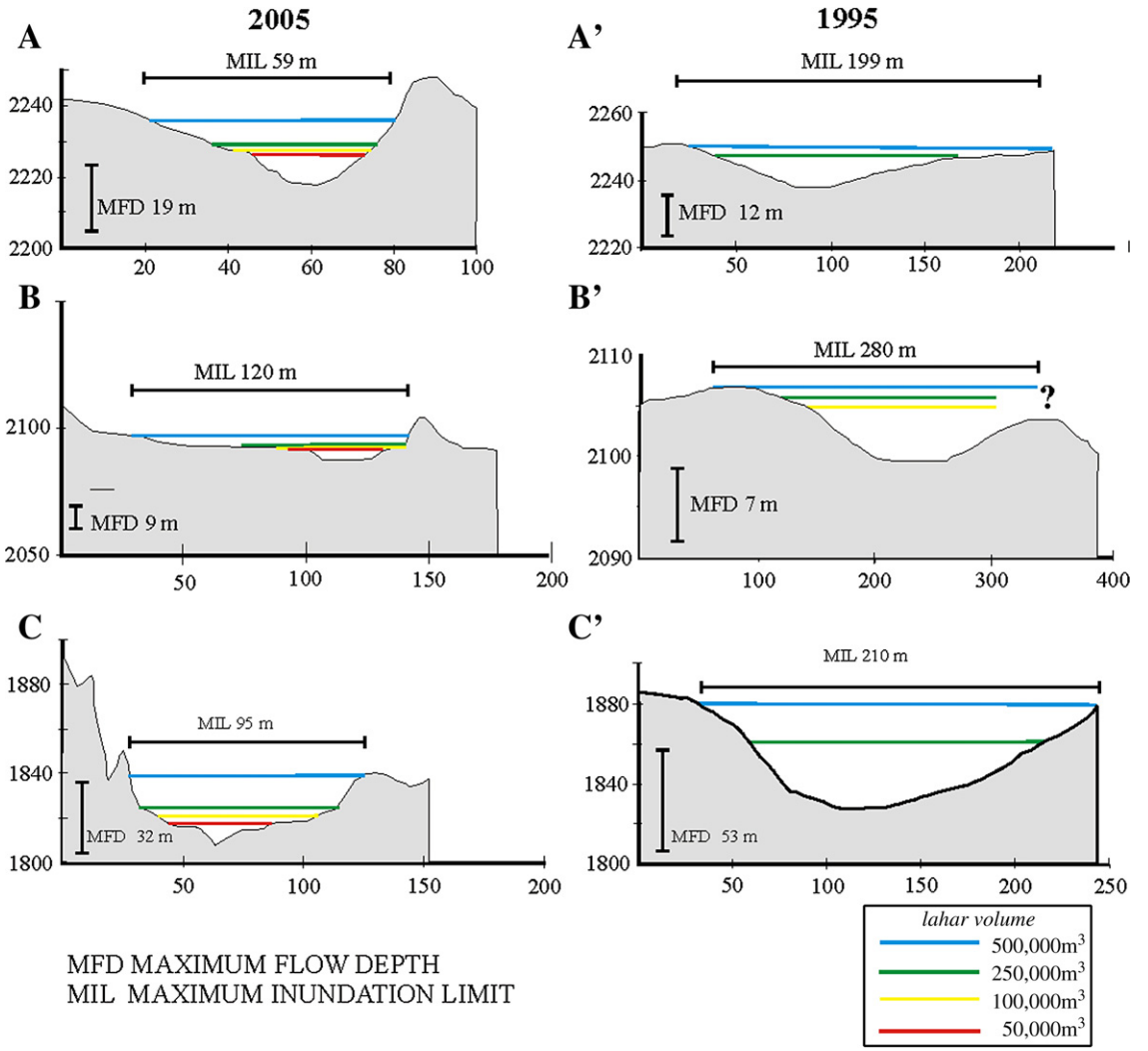

Fig. 14. Section performed on the 1995 and 2005 DEM to show the difference in inundation limits.

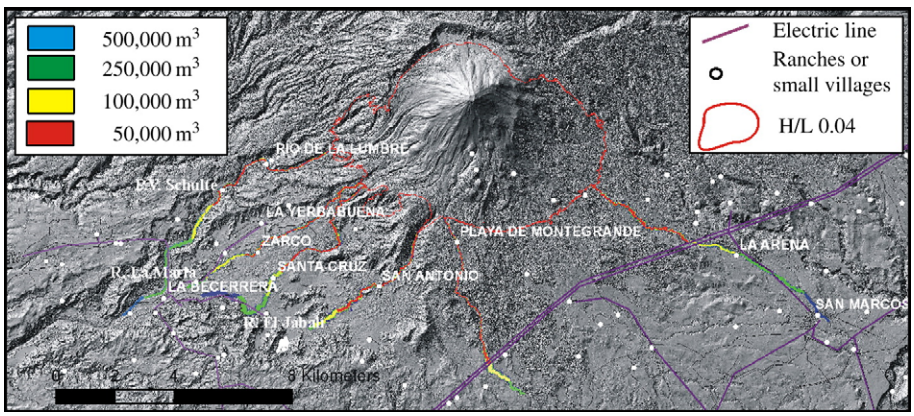

Fig. 15. Hazard map for high frequency and low magnitude lahars at Volcán de Colima. Note that several small villages can be affected by such type of flow.

for monitoring its drainage system evolution with time. For Volcán de Colima, the spectral classification helped to determine the source, path and runout of small in volume but frequent lahars that occurred during the last period of activity, useful to prepare a hazard zonation. The lahar simulation indicated that low resolution DEMs are overestimating lahar inundation limits but reducing their runout. This is an important issue since despite a good estimation of the flow volume, its simulation could be misinterpreted and the resulting hazard map could underestimate the real flow runout distance.

Acknowledgements

This work was supported by Conacyt grant (project n. 46340) and PAPIIT (no. 103107) to L. Capra, as well by Universidad de Colima's FRABA grant (project no. 430/06) to J.C. Gavilanes-Ruiz. CENAPRED (Centro Nacional de Prevencion de Desastres) kindly provided the LIDAR topography. Thanks to Gabriel Reyes for seismic data. This work benefited from constructive reviews by V. Manville and R. Saucedo.

References

Capra, L., Macías, J.L., 2002. The cohesive Naranjo debris flow deposit (10 km^3): a dam breakout flow derived from the Pleistocene debris-avalanche deposit of Nevado de Colima volcano (México). Journal of Volcanology and Geothermal Research 117, 213–235.

Capra, L., in press. Volcanic Natural Dams: identification, stability and secondary effects. Natural Hazards.

Cortés Cortés, Abel, Garduño-Monroy, V.H, Navarro, C., Komorowski, J.-C., Saucedo, R., Macías, J.L., y Gavilanes, J.C., 2005. Carta Geológica del Complejo Volcánico de Colima, Con Geología del Complejo Volcánico de Colima. CARTAS GEOLÓGICAS Y MINERAS0185-4798, vol. 10.

Gavilanes-Ruiz, J.C., 2004. Simulación de escenarios eruptivos del volcán de Colima y aportaciones al plan de contingencias del estado de Colima. Facultad de Filosofia y Letras. UNAM, Mexico DF. 156 pp.

Gudmundsson, M.T., Sigmundsson, F., BjÃrnsson, H., 1998. Ice-volcano interaction on the 1996 Gjalp suclacial eruptio, Vatnajokul, Iceland. Nature 389, 954–957.

Kauth, R.J., Lambeck, P.F., Richardson, W., Thomas, G.S., Pentland, A.P., 1979. Feature Extraction Applied to Agricultural Crops as Seen by Landsat. Proceedings, LACIE Symposium, Houston TX. NASA, pp. 705–721.

Komorowski, J.C., Navarro, C., Cortes, A., Saucedo, R., Gavilanes, J.C., Siebe, C., Espíndola, J.M., Rodriguez-Elizarrarás, S.R., 1997. The Colima Volcanic Complex. Fiel guide #3, IAVCEI, General Assembly, Puerto Vallarta, Mexico.

Iverson, R.M., Schilling, S.P., Vallance, J.W., 1998. Objective delineation of lahar-inundation hazard zones. Geological Society of America Bulletin 110 (8), 972–984.

Lavigne, F., Thouret, J.C., 2002. Sediment transport and deposition by rain-triggered lahars at Merapi Volcano, Central Java, Indonesia. Geomophology 49, 45–69.

Luhr, J.F., Prestegaard, K.L., 1985. Caldera formation at Volcán de Colima, México: a large Mount St. Helens-type avalanche event 4300 years ago, AGU, Fall Meeting. Eos, Transaction. American Geophysical Union, San Francisco, p. 411.

Major, J.J., Janda, R.J., Daag, A.S., 1996. Watershed disturbance and lahars on the east side of Mount Pinatubo during the mid-June 1991 eruption. In: Newhall, C., Punongbayan, R.S. (Eds.), Fire and Mud, Eruptions and Lahars of Mount Pinatubo, Phillipines. University of Washington Press, Seattle, pp. 895–919.

Manville, V., White, J.D.L., Houghton, B.F., Wilson, C.J.N., 1999. Paleohydrology and sedimentology of a post-1.8 ka breakout flood from intracaldera Lake Taupo, North Island, new Zealand. Geological Society of America Bulletin 111, 1435–1447.

Pierson, T.C., Scott, K.M., 1985. Downstream dilution of a lahar: transition from debris flow to hyperconcentrated streamflow. Water Resources Research 21 (10), 1511–1524.

Robin, C., Mossand, P., Camus, G., Cantagrel, J.-M., Gourgaud, A., Vincent, P.M., 1987. Eruptive history of the Colima volcanic complex (Mexico). Journal of Volcanology and Geothermal Research 31, 99–113.

Rodolfo, K.S., Arguden, A.T., 1991. Rain-lahar generation and sedimentation-delivery systems at Mayon Volcano, Philippines. In: Fisher, R.V., Smith, G.A. (Eds.), Sedimentation in volcanic settings. SEPM Special Publication, pp. 71–87.

Sarocchi, D. 2006. Análisis textural del depósito de bloques y ceniza del 17 de julio de 1999 en el Volcán de Colima. Universidad Nacional Autónoma de México, Instituto de Geofísica, Mexico City, PhD Thesis, 222 pp.

Saucedo, R., Macias, J.L., Bursik, M.I., Mora, J.C., Gavilanes, J.C., Cortes, A., 2002. Emplacement of pyroclastic flows during the 1998–1999 eruption of Volcan de Colima, Mexico. Journal of Volcanology and Geothermal Research 117 (1–2), 129–153.

Saucedo, R., Macias, J.L., Bursik, M.I., 2004. Pyroclastic flow deposits of the 1991 eruption of Volcán de Colima, México. Bulletin of Volcanology 66, 291–306.

Saucedo, R., Macias, J.L., Sheridan, M.F., Bursik, M.I., Komorowski, J.C., 2005. Modeling of pyroclastic flows of Colima Volcano, Mexico; implication for hazard assessment. Journal of Volcanology and Geothermal Research 139 (1–2), 103–115.

Schilling, S.P., Iverson, R.M., 1998. Automated, reproducible delineation of zones at risk from inundation by large volcanic debris flow. Proc. FirstInt. Conf. on Debris Flow Hazards Mitigation, San Francisco, USA. ASCE, pp. 176–186.

Scott, K.M., 1988. Origins, behaviour, and sedimentology of lahars and lahar-runout flows in the Toutle-Cowlitz River System. U.S. Geological Survey Professional Paper, vol. 1447-A. 74 pp.

Smith, G.A., Fritz, W.J., 1989. Volcanic influences on terrestrial sedimentation. Geology 17, 375–376.

Stevens, N.F., Manville, V., Heron, D.W., 2002. The sensitivity of a volcanic flow model to digital elevation model accuracy: experiments with digitized map contours and interferometric SAR at Ruapehu and Taranaki volcanoes, New Zealand. Journal of Volcanology and Geothermal Research 119, 89–105.

Stoopes, G.R., Sheridan, M.F., 1992. Giant debris avalanches from the Colima Volcanic Complex, Mexico: implication for long-runout landslides (>100 km). Geology 20, 299–302.